Transport coefficients of hard-sphere mixtures. III. Diameter ratio 0.4 and mass ratio 0.03 at high fluid density

Jerome J. Erpenbeck
Los Alamos National Laboratory, Los Alamos, New Mexico 87545
(Received 1 March 1993)

The equation of state and the transport coefficients of shear viscosity, thermal conductivity, thermal diffusion, and mutal diffusion are estimated for a binary, equimolar mixture of hard spheres having a diameter ratio of 0.4 and a mass ratio of 0.03 at volumes in the range $1.7V_0$ to $3V_0$ ($V_0 = \frac{1}{2}\sqrt{2}N\sum_a x_a \sigma_a^3$, where x_a are the mole fractions, σ_a are the diameters, and N is the number of particles), complementing and, in some cases, improving earlier low-density results through Monte Carlo, molecular-dynamics calculations using the Green-Kubo formulas. Calculations are reported for 108 to 2048 particles, so that both finite-system and, in the case of the transport coefficients, long-time tail corrections can be applied to obtain accurate estimates of the pressure and the transport coefficients in the thermodynamic limit. Corrections of both types are found to be increasingly important at higher densities, for which the pressure is observed to become nonlinear in $1/N$ over the range covered. The Mansoori-Carnahan-Starling-Leland (MCSL) equation is found to account for the pressure with considerable accuracy for $V \geq 1.7V_0$; the difference between the observed (infinite-system) pressure and the MCSL prediction increases monotonically with density, reaching 0.4% at $V = 1.7V_0$. For volumes below $2V_0$ the pressure in excess of the MCSL prediction is found to "soften" slightly in its dependence on the density. The pressure is also compared with the known virial series (B_2 and B_3) and the difference is fitted to a rational polynomial from which estimates for B_4 and B_5 are derived. The transport coefficients are compared with the predictions of the revised Enskog theory, evaluated using the MCSL equation of state. The shear viscosity coefficient is found to lie within about 5% of the theory over much of the range of densities, exceeding the Enskog prediction at both high and low densities and rising sharply at the highest densities. The thermal conductivity drops to about 94% of the Enskog value at about $2.5V_0$, but the ratio increases at higher densities. The thermal diffusion and mutal diffusion coefficients, relative to the Enskog values, drop monotonically to roughly 0.75 with increasing density. The pressure estimates vary in accuracy from 0.001% to 0.01% with increasing density. The accuracy of the estimates of the transport coefficients similarly ranges from 0.5% to 3.8%. The magnitude of the $1/N$ corrections to both the pressure and the transport coefficients increase with density, equaling, for example, 0.3% of the 256-particle pressure at $V = 1.7V_0$. At the same density, the combined finite-system and long-time tail correction for the mutual diffusion is 4.3% of the 256-particle result.

PACS number(s): 51.10.+y, 05.60.+w, 66.10.−x, 66.20.+d

I. INTRODUCTION

The prediction of the thermophysical properties of matter from knowledge of the microscopic interaction potential remains the central objective of statistical mechanics. While the exact theory can be carried quite far in the low-density limit, the extension to liquid densities has been painstakingly difficult for the transport properties compared to the successful treatment of the equation of state. The latter has proceeded through both systematic and *ad hoc* analytic theory combined with numerical simulation via Monte Carlo and molecular dynamics. For the transport coefficients, however, the situation for dense fluids remains problematic. The *ad hoc* generalization of the Boltzmann theory for high-density hard spheres by Enskog [1,2] (along with recent extensions) remains virtually the only analytic calculation of transport coefficients. The systematic extension of the Boltzmann equation to finite densities reveals divergences in the density series [3,4] unlike the well-behaved virial series for the pressure. While it is possible to at least par-

tially renormalize the theory through summation of the so-called ring events, that path has been limited by the difficulty of the calculation to the determination of the long-time tails of the Green-Kubo time-correlation functions [5,6]. Similarly, the cutoff of the divergent integrals which arise in the density series through mean-free-path arguments yields at most the first few terms for the hard-sphere fluid [7,8]. Alternatively, the application of hydrodynamics at the microscopic level to the evaluation of the time-correlation functions of the Green-Kubo theory, which yields long-time tails in agreement with the kinetic theory [9,10] has gained importance in the theory of transport.

The paucity of theoretical results creates a need for hard results against which theoretical advances can be tested. Indeed, the evaluation of transport coefficients for simple interaction potentials is important both from the point of view of theory and also in providing a guide to experiment where it is important that the behavior of idealized substances be known if one is to interpret effects arising from the more complicated aspects of the interac-

tion potential. While there exist many such results in the literature for single-component fluids, there are few extant results for mixtures. The present series of papers attempts to fill this niche through evaluation of both the equation of state and the transport coefficients of binary hard-sphere mixtures at densities in the fluid regime.

In the preceding papers [11,12] of this series, we have compared the transport coefficients of binary hard-sphere mixture estimated through Monte Carlo (MC), molecular-dynamics (MD) calculations with the predictions of the revised Enskog theory [13–18]. In I, for the case of a binary, equimolar, "isotopic" mixture having a mass ratio 0.3 and a volume of $3V_0$,

$$V_0 = \frac{1}{2}\sqrt{2}N \sum_{a=1}^{n_s} x_a \sigma_a^3 \tag{1}$$

[in which n_s is the number of components (2, in the present case), N is the total number of particles in the system, and x_a and σ_a are the mole fraction and hard-sphere diameter of species a, respectively] we found the "thermal" transport coefficients of thermal conduction and mutual and thermal diffusion to exceed the theoretical predictions by from 11% to 22%, even though the shear viscosity was less than 2% high. In II, we considered a helium-xenonlike mixture having a diameter ratio of 0.4 and a mass ratio of 0.03 at low densities, viz. from $5V_0$ to $20V_0$. Deviations from the Enskog theory were found to be *negative* for the thermal transport properties and positive for the shear viscosity, although not strongly so. Over the density range treated, the deviations were all less than 6%.

In the present paper we extend the study of the latter system to higher densities by treating volumes in the range $3V_0$ to $1.7V_0$. Because this range lies well above that for the fluid-solid phase transition for the single-component fluid ($\sim 1.5V_0$), the mixture is expected to remain stable against solidification throughout. However, the possibility of other phase transitions, for example, fluid phase separation, within this interval is not so easily dismissed. A number of MC and MD calculations have studied hard-sphere mixtures having similar diameter ratios: equimolar mixtures having a diameter ratio of $\frac{3}{5}$ and $V > 1.57V_0$ by Smith and Lea [19], equimolar mixtures having a diameter ratio of $\frac{1}{3}$ and $V > 1.46V_0$ by Adler [20], an equimolar mixture with diameter ratio 0.3 and $V = 1.51V_0$ by Lee and Levesque [21], mixtures having diameter ratios of $\frac{1}{2}$ and $\frac{1}{3}$ and $1.65V_0 < V < 1.26V_0$ by Fries and Hansen [22] at several low concentrations of the larger spheres, and mixtures having diameter ratios of $\frac{1}{3}$ and $\frac{3}{5}$ and $V > 1.23V_0$ at three values of the mole fraction, including the equimolar case, by Jackson, Rowlinson, and van Swol [23]. Attention is also drawn to the MC and MD studies by Kranendonk and Frenkel [24,25] directed at eliciting the phase diagram of binary hard-sphere mixture for diameter ratios near 1. In each of these studies, the authors report the existence of a stable solid phase only for volumes less than the hard-sphere fluid-solid transition, $V \sim 1.5V_0$, with no evidence for the appearance of coexisting fluid phases. Indeed, until recently, the possibility of demixing into two fluid phases

has been widely discounted on the basis of both these results and the predictions of the Percus-Yevick integral equation [26,27]. Recently, however, Biben and Hansen [28] have, on the basis of an improved theory, argued for the existence of phase separation for diameter ratios below 0.2. Moreover, Frenkel and Louis [29] have proven that phase separation occurs in the absence of attractive interaction for certain lattice mixtures. Thus the exact nature of the phase diagram for hard-sphere mixtures remains conjectural, particularly for diameter ratios well below 1.

We study, then, the equation of state with some care, including the dependence on system size, comparing the pressure and the mean free time with the predictions of the Mansoori-Carnahan-Starling-Leland [30,31] (MCSL) theory, which is widely believed to improve upon the Percus-Yevick equation of state, whether from the compressibility or the virial expression. Because our primary interest here concerns the transport coefficients and these require a more thorough exploration of phase space than the equation of state to achieve a given accuracy, the present calculations are considerably more precise with respect to the equation of state than those previously reported. At the highest densities studied, the statistical uncertainties in the pressure are sufficiently precise as to reveal the nonlinearity in its dependence on the reciprocal of the number of particles, with the large-N linear dependence becoming steeper and moving to larger N, beyond the 108-particle regime.

In our study of the transport coefficients, we compare our results with the predictions of the revised Enskog theory. Our calculations include long-time tail corrections to the Green-Kubo expressions for the transport properties as well as finite-system-size corrections. Indeed, one objective of the present study is the determination of the importance of these corrections over a broad range of densities in the face of the fact that most of the literature on the simulation of the thermophysical properties ignore them. Here we find small but significant corrections of each type which increase in importance with increasing density.

Some discussion of the numerical method employed is given in Sec. II. The results for the pressure and the mean free time are discussed in Sec. III and the values are extrapolated to the thermodynamic limit. The latter are compared with the MCSL theory and the virial series. Estimates for the fourth and fifth virial coefficients are presented. In Sec. IV, the analogous procedures and results for the transport coefficients are described. In Sec. V we discuss the significance of our results.

II. SYSTEM AND METHODS

We consider mixtures of hard spheres, fully described in I and II, which the reader should consult for further details. Here we consider equimolar binary mixtures in which the particles of species 2 have diameter $0.4\sigma_1$ and mass $0.03m_1$, values similar to those for helium-xenon mixtures. While the pressure is independent of the mass ratio, the transport coefficients are not.

For each of six values of the volume in the interval

$[3V_0, 1.7V_0]$ we have calculated the transport coefficients, as previously described, and the equation of state for a fixed set of five system sizes, viz. 108, 256, 500, 864, and 1372 particles; the exceptions are the volume $3V_0$ for which the 256-particle system was not considered and the volume $1.7V_0$ for which a calculation for 2048 particles was added. For each N and V, the calculation consists of a MC random walk in configuration space in which at least 200 attempts to "move" each of $N-1$ particles were made in generating the ith configuration $\mathbf{r}_i^N$ from the $(i-1)$th. The ith point in phase space $\mathbf{x}_i^N$ is then formed from $\mathbf{r}_i^N$ and a point in momentum space $\mathbf{p}_i^N$ chosen randomly and uniformly from the "molecular-dynamics" ensemble distribution function for composition $\mathbf{N} = (N_1, N_2, \dots, N_{n_s})$, volume V, energy E, and linear momentum $\vec{\mathbf{M}}$,

$$\rho(\mathbf{N}VE\vec{\mathbf{M}}) = \frac{\delta(H_N(\mathbf{p}^N) - E)\delta(\vec{\mathbf{P}}_N(\mathbf{p}^N) - \vec{\mathbf{M}})}{Z(\mathbf{N}VE\vec{\mathbf{M}})} ,$$

$$Z(\mathbf{N}VE\vec{\mathbf{M}}) = \int d\mathbf{r}^N \int d\mathbf{p}^N \delta(H_N(\mathbf{p}^N) - E)$$
$$\times \delta(\vec{\mathbf{P}}_N(\mathbf{p}^N) - \vec{\mathbf{M}}) , \qquad (2)$$

in which H_N is the Hamiltonian, $\mathbf{P}_N$ is the total momentum of the system, and $\delta(x)$ denotes the delta function of the dimensionality of its argument. For the case of $\vec{\mathbf{M}} = \vec{0}$ which we treat, the selection of momenta is made using the Box-Muller [32] method to yield raw velocities $\vec{v}_i$ from the Maxwell-Boltzmann distribution for temperature T given by

$$\beta = \frac{1}{k_B T} = \frac{3(N-1)}{2E} , \qquad (3)$$

which are then translated to the center-of-mass frame of reference and scaled to the desired energy surface to yield the momenta

$$\vec{p}_i = f m_{s_i} (\vec{v}_i - \vec{v}) ,$$

$$\vec{v} = \frac{\sum_i m_{s_i} \vec{v}_i}{\sum_a N_a m_a} , \qquad (4)$$

$$f = \left[\frac{E}{\frac{1}{2} \sum_i m_{s_i} (\vec{v}_i - \vec{v})^2} \right]^{1/2} ,$$

in which the a sums extend over species and the i sums extend over particles. Each of the MC phase points $\mathbf{x}^N = (\mathbf{r}^N, \mathbf{p}^N)$ so selected is used as the initial phase for a dynamical trajectory on which we compute the pressure, the collision rate, and the transport coefficients. For the calculations reported here, each trajectory was developed to a time of $6000t_{00}$, where t_{00} is the Boltzmann expression for the mean free time, as given in II. For each (V,N) pair, 50 such trajectories were generated in the combined MC and MD calculation; the exceptions are the $V = 3V_0$ realizations for $N = 108$, 864, and 1372 which have 30 trajectories and the $V = 1.7V_0$, $N = 2048$ case with 27 trajectories. Because the ratio of the actual mean free time to the Boltzmann value decreases with decreasing volume, the total number of collisions calculated for given values of V and N varies between the 1.8×10^7 collisions for 108 particles at $3V_0$ and the 7.0×10^8 for 1372 particles at $1.7V_0$.

In addition to the standard Metropolis algorithm to generate the set of configurations $\{\mathbf{r}_i^N\}$, we also use a variant in which the final configuration from the ith MD trajectory becomes the starting configuration for $(i+1)$th set of MC moves. In those cases in which our 200 (or more) MC steps seem inadequate to destroy all traces of serial correlation, viz. at high density, this "augmented" method appears to be advantageous. A second variant in the Monte Carlo algorithm was employed in one case, viz. the interchange of a larger with a smaller particle using the method of Kranendonk and Frenkel [24]. One such interchange was attempted following the attempt to move each of the particles once by the Metropolis method.

The initial configuration for these calculations was (i) for $V \geq 1.9V_0$, the face-centered cubic (fcc) lattice with the two species randomly distributed over the sites or (ii) for $V \leq 1.8V_0$, the final configuration achieved on one of the trajectories of the adjacent lower-density realization having the same value of N uniformly compressed to the smaller volume in steps dictated by the nearest pair of particles after a series of ten MC moves per particle at the current volume. However, for $V = 1.7V_0$, $N = 2048$, the initial configuration was constructed from eight appropriately translated images of a configuration from the $N = 256$ calculation at the same reduced volume. These techniques were invoked because for volumes less than $[2/(1 + 0.4^3)]V_0 \approx 1.88V_0$ the separation of nearest-neighbor sites of the fcc lattice is less than the diameter of the larger particles. Because of the length of the MC step and, particularly, the MD trajectory, we have observed no significant initial transient in the observations, irrespective of V, for the augmented MC algorithm. For cases in which we have employed the standard algorithm, only for high densities do we find evidence for serial correlation of our results. For reduced volumes of 2 and 1.9, we find that values of the acceptance-to-rejection ratio of MC moves are serially correlated for the first several cycles of the calculation. Nonetheless, the trajectory averages which enter the equation of state and the transport coefficients show no correlations over the corresponding trajectories. Thus, even though the augmented algorithm would have been preferred for these values of V as well, it seems clear that our trajectories are sufficiently long that the correlations are limited to the initial portion of these trajectories and the trajectory averages show no appreciable trace thereof.

We also recognize the recent study of Ferrenberg, Landau, and Wong [33], which demonstrates the failure of MC calculations to yield correct results for the equation of state of the two-dimensional Ising model under various combinations of algorithms and pseudo-random number generators. While the present calculations are far more extensively time averaged than they are phase-space averaged, under the circumstance it seems appropriate to detail our use of pseudo-random-number generators. In the

generation of each realization of the Markov chain in configuration space, we employ a different random-number generator for each spatial component of the particle displacements. Another pair of generators are used in applying the Box-Muller algorithm in obtaining the particle velocities. Finally, a sixth generator is used to set up the initial fcc lattice configuration in choosing randomly the species label of the particle at each lattice site. For $V \leq 1.8 V_0$, for which case initialization uses a configuration achieved for a larger V, this generator is not used. The set of generators for each particular pair of N, V values were chosen from the 48-bit generators, $M20$, $M21$, and $M40$, described by Wood [34], with the particular choice of generators and the portion of the 2^{46} (or 2^{48} for the $M21$ generator) period of each generator used varied from state point to state point. Because the number of random variates from any one sequence was typically no more than $50 \times 1372 \times 200 \sim 14 \times 10^6$ (i.e., 50 trajectories, 1372 or fewer particles, and usually 200 attempted moves per particle), we employed only a small fraction of each of the random-number sequences.

While the pressure was calculated in our earlier work (I and II), neither the results nor the method of its calculation were described. The pressure is obtained through the virial, as discussed by Erpenbeck and Wood [35]; for each trajectory we obtain an estimate

$$p = \frac{2[E - \overline{W}(t_f)]}{3V},$$

$$\overline{W}(t) = -\frac{1}{2t} \sum_{\gamma=1}^{c(t)} \vec{\sigma}_{ij}(t_\gamma) \cdot \Delta \vec{p}_i(t_\gamma),$$

(5)

in which t_f is the length of the trajectory (here, $6000 t_{00}$), the overbar denotes a time average, W is the virial, $c(t)$ is the number of collisions up to time t, the γ sum is over the times $t_1, t_2, \ldots,$ of the successive collisions, $i(\gamma), j(\gamma)$ denote the pair involved in the γth collision, $\vec{\sigma}_{ij} = \vec{r}_i(t_\gamma) - \vec{r}_j(t_\gamma)$ denotes the line of centers at the time of collision, and $\Delta \vec{p}_i$ denotes the momentum change of particle i on collision γ. The collection of 50 values of the pressure, one from each trajectory, yields then the average pressure and its statistical uncertainty. The standard tests of statistical quality described in II are applied to assure us of the absence of measurable correlations between successive trajectories and hence the reliability of our estimate for the statistical uncertainty.

In addition to the 30 systems treated in the $[3V_0, 1.7V_0]$ range of volumes, we have also extended many of the low-density calculations reported in II by adding calculations for system sizes not previously studied or repeating calculations reported there, but now extending these to the trajectory lengths and numbers of trajectories used here. Indeed, most of the calculations reported here were executed with an entirely new version of the computer program. Development of the latter revealed a discrepancy in the definition of the temperature in terms of the energy, Eq. (3), whereby the old program replaced the $N - 1$ term in that definition by N, contrary to the assertion in II. As a result, the old results need to be corrected by a factor of $[(N-1)/N]^{n/2}$, with the value of n dependent on the particular quantity in ques-

tion: (i) for the mean free time $n = -3$, (ii) for the mutual diffusion coefficient $n = 1$, (iii) for the shear viscosity and the thermal diffusion coefficient $n = 3$, and (iv) for the thermal conductivity $n = 5$. The values reported for the thermodynamic limit are, of course, independent of these corrections, provided either one or the other choice for the $\beta - E$ relation is adopted for a given density.

Finally, we correct our expression for the mean free time [given incorrectly in Eq. (77) of I]. If we denote the number of collisions observed on a trajectory as $c(t_f)$ (in which t_f is the final time $6000 t_{00}$ for the trajectory), then the mean free time for that trajectory is

$$t_0 = \frac{t_f N}{2c(t_f)}.$$

(6)

The average of these values over trajectories yields the values reported below.

III. EQUATION OF STATE

The systems studied, including the extended low-density ones, are listed in Table I, which also specifies the nature of the MC algorithm used. The table also lists results for the compressibility factor $Z = pV/Nk_B T$ and the mean free time t_0, including the modified results for t_0 from II.

In order to obtain the equation of state in the thermodynamic limit, we plot the reduced pressure $\phi = pV_0/Nk_B T$, less the MCSL theory prediction, as a function of $1/N$ in Fig. 1 for $V \leq 3V_0$. The behavior displayed for $2.4V_0$ and $3V_0$ is typical of the low-density results in that the data are consistent with a linear extrapolation to the infinite-system limit. At higher densities, however, we see that the 108-particle and even the 500-particle (at $1.7V_0$) pressures are inconsistent with a linear dependence in $1/N$. Fitting the data on the linear portion by weighted linear least squares, we extrapolate to $N = \infty$ to obtain the values of the compressibility factor given in Table I. We note that the 2048-particle result for $1.7V_0$ suggests the displayed fit in which the 108- to 500-particle points are omitted, leading to the continued increase of the slope of the $1/N$ line with density. The calculated infinite-system pressure is plotted in the form of $\Delta\phi = \phi - \phi^{MCSL}$ as a function of reduced density in Fig. 2, which also shows the mean-free-time difference $\Delta t_0 = t_0 - t_0^{MCSL}$. We note that the deviations from the theory for both ϕ and t_0 grow rapidly with density, but remains less than 0.7% over the entire range. We also note that the change in N dependence seen in Fig. 1 correlates with a slight "softening" in the pressure difference for V below $2V_0$. While the magnitude of this change in slope of the pressure is small, it appears to be significant. Finally, we note that the apparent change of sign of Δt_0 at low density, discussed in II, is of marginal statistical significance in the light of the improved results presented here.

It should not be supposed that the decrease in slope of $\Delta\phi$ near $V = 1.8V_0$ in Fig. 2(a) represents a softening of the equation of state, i.e., an increase in the isothermal compressibility. Because the figure shows a difference in
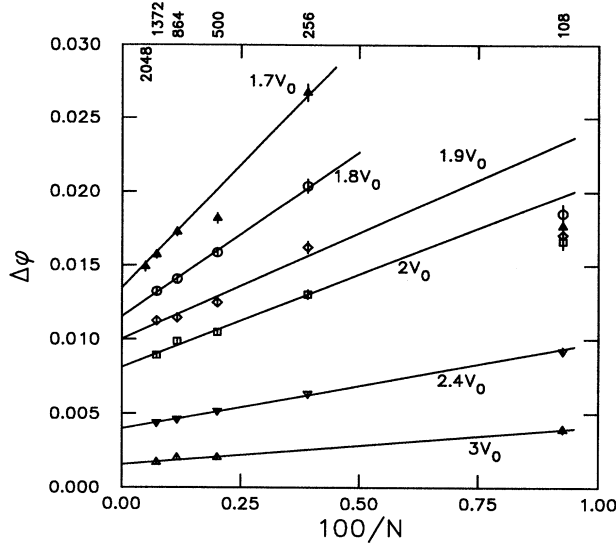
FIG. 1. Deviation $\Delta\phi$ of the reduced pressure pV_0/Nk_BT from the MCSL prediction as a function of the number N of particles at volumes of $3V_0$ (triangle, point up), $2.4V_0$ (triangle, point down), $2V_0$ (square), $1.9V_0$ (diamond), $1.8V_0$ (circle), and $1.7V_0$ (filled triangle). The lines are weighted least-square fits to the $N>500$ data for $1.7V_0$, the $N\geq256$ data for $1.8V_0\leq V\leq2V_0$, and to all values of N for $V\geq2.4V_0$. Statistical uncertainties are marked at plus or minus one standard deviation.

pressures, the decrease in slope only indicates a change relative to the MCSL pressure. The value of $[\partial\phi/\partial(V_0/V)]_T$ in fact appears to increase with increasing density throughout the range of densities reported here.

It is also interesting to compare the observed pressure with the virial series,

$$Z=1+\sum_{n=1} B_{n+1}\left[\frac{N}{V}\right]^n .\qquad(7)$$

The second and third virial coefficients have been evaluated exactly by Kihara [36,37] for mixtures of square-well particles. For hard spheres, these reduce to

$$B_2=\frac{2\pi}{3}\sum_{i,j=1}^{n_s} x_ix_j\sigma_{ij}^3 ,$$

$$B_3=\left[\frac{2\pi}{3}\right]^2\sum_{i,j,k=1}^{n_s} x_ix_jx_kB_3^{(ijk)} ,$$

$$B_3^{(iii)}=\frac{5}{8}\sigma_{ii}^6 ,\qquad(8)$$

$$B_3^{(iij)}=\frac{\sigma_{ii}^3-18\sigma_{ii}\sigma_{ij}^2+32\sigma_{ij}^3}{24}\sigma_{ii}^3 ,$$

in which $B_3^{(ijk)}$ is independent of permutations of the superscripts. The fourth virial coefficient has been evaluated explicitly only for diameter ratios of $\frac{3}{5}$ and $\frac{1}{3}$ [38].

The agreement of our data with the known virial coefficients is demonstrated in Fig. 3 in which we plot $\Delta_v\phi=(Z-Z_3^{(v)})(V/V_0)^3$, in which $Z_n^{(v)}$ denotes the virial series including terms through B_n, as a function of density. Fitting the function $F(V_0/V)=(Z-Z_2^{(v)})/[B_3(V_0/V)^2]$ to various rational functions,

$$[p/q]=\frac{N_p(V_0/V)}{D_q(V_0/V)} ,$$

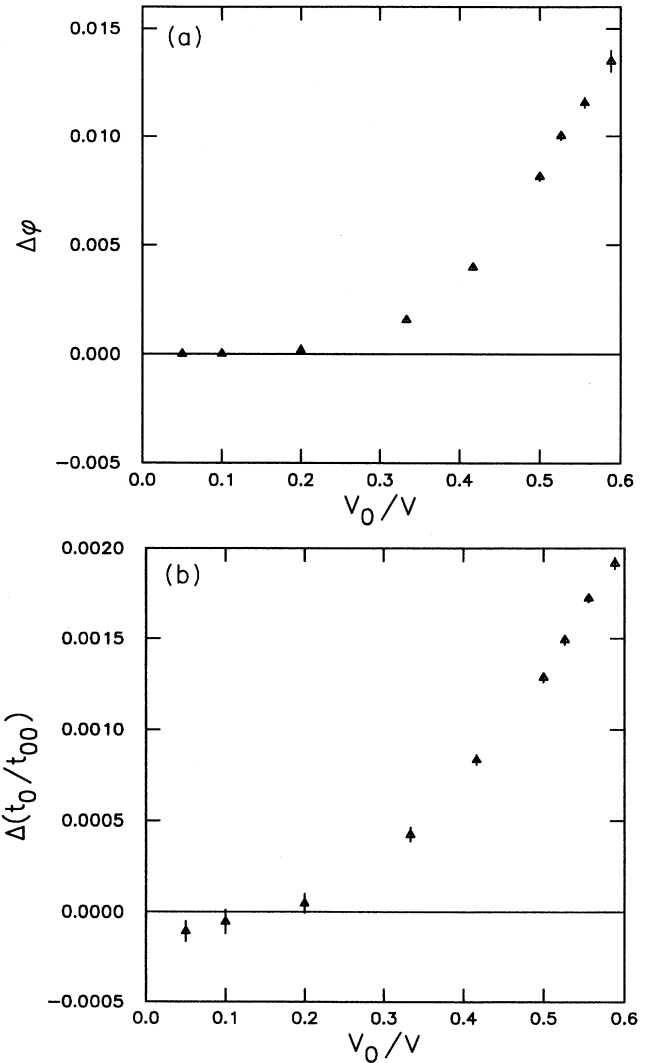$$N_p(x)=1+\sum_{n=1}^p P_nx^n ,\qquad(9)$$

$$D_q(x)=1+\sum_{n=1}^q Q_nx^n ,$$

FIG. 2. Deviation of the equation of state from the MCSL equation of state as a function of reduced density V_0/V: (a) the reduced pressure ϕ and (b) the mean free time t_0 relative to the Boltzmann value t_{00}. Statistical uncertainties are marked at plus or minus one standard deviation.
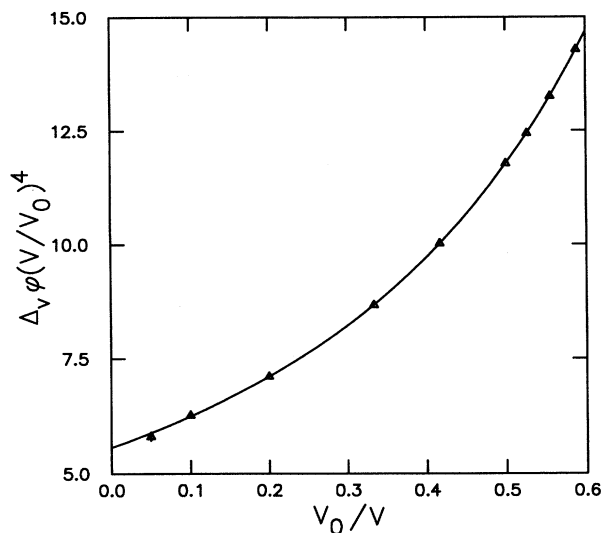
FIG. 3. Deviation $\Delta_v\phi$ of the compressibility factor from the three-term virial series as a function of reduced density V_0/V. The curve is the [3/1] rational function fit, Eq. (9), to the data, with coefficients given by Eq. (10). Statistical uncertainties are marked at plus or minus one standard deviation.

we find an adequate fit when $p=3$ and $q=1$, with

$$P_1=0.427\,614\,59 \ ,$$

$$P_2=0.220\,040\,03 \ ,$$

$$P_3=0.410\,946\,30 \ ,$$

$$Q_1=-0.901\,140\,79 \ ,$$

(10)

with a goodness of fit $\chi^2=2.6$ for five degrees of freedom. The fit is also plotted in Fig. 3. Our estimates for the fourth and fifth virial coefficients are derived from Eqs. (7)–(9) to be

$$B_4=\left[\frac{2\pi V_0}{3N}\right]^3 (0.606\pm0.002) \ ,$$

$$B_5=\left[\frac{2\pi V_0}{3N}\right]^4 (0.309\pm0.008) \ ,$$

(11)

in which the "uncertainties" simply reflect the numerically observed variation in the B_n subject to several variations in the equation of state within its standard deviations.

TABLE I. Parameters and equation-of-state results for Monte Carlo and molecular-dynamics calculations in the molecular-dynamics ensemble. The volume V is given relative to a reference volume V_0, Eq. (1); N is the total number of particles, MC indicates whether the standard (s), augmented (a), and/or species-interchange (x) Monte Carlo algorithm was used, p is the pressure, k_B is the Boltzmann constant, T is the temperature, Eq. (5), t_0 is the mean free time, and t_{00} is the Boltzmann mean free time. The asterisks mark realizations reported in II.

$\dfrac{V}{V_0}$	N	MC	$\dfrac{pV}{Nk_BT}$	$\dfrac{t_0}{t_{00}}$	$\dfrac{V}{V_0}$	N	MC	$\dfrac{pV}{Nk_BT}$	$\dfrac{t_0}{t_{00}}$
1.7	108	a	6.797 5(14)	0.296 026(60)		864	s	3.468 92(25)	0.462 419(38)
	256	a	6.812 9(10)	0.295 746(40)		1372	s	3.468 36(19)	0.462 308(29)
	500	a	6.798 34(56)	0.295 429(25)		∞		3.467 38(17)	0.462 175(26)
	864	a	6.796 76(45)	0.295 312(20)	3	108	s	2.606 26(75)	0.558 435(15)
	1372	a	6.794 72(33)	0.295 285(17)		500	s	2.600 60(24)	0.556 177(57)
	2048	ax	6.792 74(53)	0.295 249(16)		864	s	2.600 53(23)	0.555 890(47)
	∞		6.790 36(83)	0.295 208(30)		1372	s	2.599 59(17)	0.555 740(44)
1.8	108	a	5.931 4(11)	0.325 221(56)		∞		2.599 20(16)	0.555 523(38)
	256	a	5.934 74(82)	0.324 879(51)	5	108	s	1.713 60(24)	0.724 708(180)
	500	a	5.926 61(53)	0.324 556(25)		500	s	1.712 23(9)	0.721 220(96)
	864	a	5.923 38(39)	0.324 436(23)	*	500	s	1.712 53(22)	0.721 094(165)
	1372	a	5.921 87(35)	0.324 425(15)		864	s	1.711 93(10)	0.720 862(63)
	∞		5.918 83(42)	0.324 310(19)	*	1372	s	1.711 79(8)	0.720 735(64)
1.9	108	a	5.269 4(12)	0.352 639(79)		∞		1.711 71(7)	0.720 343(52)
	256	a	5.267 75(76)	0.352 046(57)	10	108	s	1.291 87(10)	0.861 801(240)
	500	s	5.260 64(45)	0.351 772(36)		500	s	1.291 75(5)	0.856 980(110)
	864	s	5.258 68(37)	0.351 612(24)		864	s	1.291 76(5)	0.856 296(99)
	1372	s	5.258 31(27)	0.351 513(20)	*	1372	s	1.291 80(3)	0.856 051(67)
	∞		5.255 96(35)	0.351 398(26)		∞		1.291 77(3)	0.855 562(64)
2	108	s	4.753 5(10)	0.378 169(64)	20	108	s	1.133 02(5)	0.934 541(320)
	256	s	4.746 31(59)	0.377 488(55)		256	a	1.132 94(3)	0.929 781(170)
	500	s	4.741 19(41)	0.377 028(37)		500	a	1.132 98(3)	0.928 166(160)
	864	s	4.739 96(34)	0.376 875(24)	*	500	s	1.132 92(4)	0.928 444(176)
	1372	s	4.738 09(26)	0.376 818(19)		864	s	1.132 98(2)	0.927 477(99)
	∞		4.736 48(31)	0.376 657(25)		1372	s	1.133 01(2)	0.927 245(69)
2.4	108	s	3.479 98(62)	0.464 065(96)	*	1372	s	1.133 01(2)	0.927 416(89)
	256	a	3.473 13(37)	0.463 082(71)	*	4000	s	1.133 00(3)	0.926 569(123)
	500	a	3.470 28(34)	0.462 636(46)		∞		1.133 00(1)	0.926 608(55)

IV. TRANSPORT COEFFICIENTS

The calculation of the transport coefficients has been discussed in some detail previously (see II particularly). The principal issues concern applying long-time and finite-system corrections to the time-dependent Green-Kubo transport coefficients

$$L_\alpha(t;N) = \frac{\beta}{V} \int_0^t dt' \rho_\alpha(t';N) \qquad (12)$$

for generic transport coefficient L_α. Indeed, for the most part, calculations of transport coefficients reported in the literature, whether based on the Green-Kubo formulas or on nonequilibrium molecular dynamics, ignore correc-

TABLE II. Monte Carlo and molecular-dynamics results for the transport coefficients relative to the values from the Enskog theory, $\hat{L}_\alpha^{[1]}(s_c;N)$, at the volume-dependent crossover times $t_c = s_c t_0$ as functions of the total number of particles N and the reduced volume V/V_0; $\alpha = 11$ for mutual diffusion. $\alpha = u1$ for thermal diffusion, $\alpha = uu$ for thermal conductivity, and $\alpha = \eta\eta$ for shear viscosity. The asterisk in the V column marks realizations from II. The numbers in parentheses are the standard deviations in the low-order digit.

V/V_0	N	$\hat{L}_{11}^{[1]}(s_c;N)$	$\hat{L}_{u1}^{[1]}(s_c;N)$	$\hat{L}_{uu}^{[1]}(s_c;N)$	$\hat{L}_{\eta\eta}^{[1]}(s_c;N)$
1.7	108	0.6817(61)	0.7223(140)	0.8701(80)	1.0382(87)
	256	0.6952(69)	0.7167(150)	0.9136(71)	1.0840(83)
	500	0.6858(72)	0.7244(170)	0.9340(80)	1.0855(110)
	864	0.7099(69)	0.7490(140)	0.9455(83)	1.0973(110)
	1372	0.7063(57)	0.7350(120)	0.9356(75)	1.1122(110)
	2048	0.7114(69)	0.7334(190)	0.9435(110)	1.0996(130)
1.8	108	0.7573(69)	0.7800(140)	0.8694(84)	0.9858(76)
	256	0.7406(86)	0.7568(150)	0.8960(92)	1.0253(98)
	500	0.7707(62)	0.8086(120)	0.9306(82)	1.0175(93)
	864	0.7722(76)	0.7970(160)	0.9570(100)	1.0315(94)
	1372	0.7757(78)	0.8106(140)	0.9372(79)	1.0355(97)
1.9	108	0.7701(72)	0.7767(120)	0.8654(93)	0.9722(95)
	256	0.7808(63)	0.7934(110)	0.9033(93)	0.9857(100)
	500	0.7812(78)	0.8034(130)	0.9140(82)	0.9906(78)
	864	0.7887(71)	0.8130(110)	0.9262(73)	0.9963(83)
	1372	0.7804(77)	0.7956(140)	0.9303(83)	1.0112(93)
2	108	0.7919(73)	0.7851(96)	0.8526(80)	0.9577(100)
	256	0.8047(78)	0.8176(130)	0.9043(84)	0.9625(93)
	500	0.7990(74)	0.8061(120)	0.9054(94)	0.9685(80)
	864	0.8203(82)	0.8201(130)	0.9146(84)	0.9627(89)
	1372	0.8168(68)	0.8323(110)	0.9246(77)	0.9722(78)
2.4	108	0.8658(80)	0.8536(93)	0.8660(73)	0.9289(91)
	256	0.8700(79)	0.8562(87)	0.8808(71)	0.9365(80)
	500	0.8665(79)	0.8611(110)	0.9099(81)	0.9320(88)
	864	0.8734(75)	0.8779(100)	0.9213(83)	0.9605(98)
	1372	0.8776(79)	0.8627(130)	0.9075(93)	0.9559(96)
3	108	0.8967(120)	0.8861(140)	0.8762(100)	0.9490(110)
	500	0.9131(84)	0.9084(110)	0.9179(84)	0.9660(86)
	864	0.9149(86)	0.9277(100)	0.9411(100)	0.9770(79)
	1372	0.9021(120)	0.8983(140)	0.9122(110)	0.9731(140)
5	108	0.9407(110)	0.9387(120)	0.9276(98)	0.9598(81)
	500	0.9448(90)	0.9485(100)	0.9432(82)	1.0054(73)
*	500	0.9280(90)		0.9481(150)	1.0026(160)
	864	0.9432(81)	0.9511(86)	0.9507(68)	1.0079(86)
*	1372	0.9498(120)	0.9562(130)	0.9527(100)	1.0026(83)
10	108	0.9673(93)	0.9752(110)	0.9678(95)	0.9682(87)
	500	0.9537(83)	0.9574(93)	0.9515(77)	1.0205(89)
	864	0.9857(86)	0.9861(100)	0.9747(78)	1.0077(98)
*	1372	0.9785(87)	0.9837(100)	0.9780(89)	0.9928(79)
20	108	0.9676(90)	0.9664(110)	0.9577(98)	0.9658(93)
	256	0.9974(88)	0.9888(100)	0.9831(87)	0.9979(95)
	500	0.9917(93)	1.0013(110)	1.0029(100)	0.9886(66)
*	500	0.9911(130)	0.9916(140)	0.9846(120)	0.9844(88)
	864	0.9899(89)	0.9872(100)	0.9876(89)	0.9903(93)
	1372	0.9919(94)	0.9899(120)	0.9921(110)	0.9954(83)
*	1372	0.9986(90)	0.9948(120)	0.9832(120)	0.9763(91)
*	4000	0.9504(220)	0.9647(300)	0.9746(270)	1.0172(210)

TABLE III. The thermal conductivity and shear viscosity as functions of reduced volume V/V_0. The Monte Carlo and molecular-dynamics estimates, relative to the Enskog values, are $\hat{L}_\alpha$, with $\alpha=uu$ for thermal conductivity and $\alpha=\eta\eta$ for shear viscosity; $\hat{L}_\alpha^{[2]}(s_c)$ is the long-time tail contribution from the mode-coupling theory for the crossover time $t_c=s_c t_0$, $\tilde{L}_\alpha$ is the Enskog transport coefficient reduced as in Eq. (13), $t_a=s_a^* t_0$ is the acoustic wave traversal time for the largest system studied at each volume, calculated from the Mansoori-Carnahan-Starling-Leland [30,31] equation of state. The numbers in parentheses are the standard deviations in the low-order digit.

V/V_0	s_a^*	s_c	$\hat{L}_{uu}$	$\hat{L}_{uu}^{[2]}(s_c)$	$\tilde{L}_{uu}^E$	$\hat{L}_{\eta\eta}$	$\hat{L}_{\eta\eta}^{[2]}(s_c)$	$\tilde{L}_{\eta\eta}^E$
1.7	57	68	0.9535(168)	0.0202	11.7986	1.1135(210)	0.0008	2.102 74
1.8	49	62	0.9506(81)	0.0209	10.6985	1.0326(90)	0.0012	1.726 50
1.9	49	57	0.9563(77)	0.0210	9.95251	1.0098(85)	0.0017	1.451 93
2	48	53	0.9446(76)	0.0206	9.43865	0.9731(79)	0.0022	1.245 53
2.4	46	43	0.9340(55)	0.0170	8.54857	0.9563(62)	0.0048	0.779 636
3	43	36	0.9431(68)	0.0110	8.42701	0.9856(66)	0.0090	0.504 468
5	34	28	0.9558(55)	0.0031	9.16589	1.0277(59)	0.0135	0.283 077
10	24	23	0.9689(57)	0.0006	10.1739	1.0168(60)	0.0067	0.214 468
20	23	22	0.9953(55)	0.0001	10.7744	0.9953(45)	0.0020	0.198 633

tions of both types. Here we follow II in choosing a crossover time t_c for which the infinite-system limit of the observed time-correlation function is joined with the mode-coupling result [39,40] for the long-time tail of the correlation function. In each case we choose t_c approximately equal to the acoustic-wave traversal time t_a for the largest system treated, viz. $N=1372$ in the present series of calculations and up to $N=4000$ for the lower densities. The values $\hat{L}_\alpha^{[1]}(t_c/t_0;N)$ of the finite-time contributions, reduced by the Enskog value L_α^E, are listed in Table II for each system size and for each transport coefficient. The values of t_a calculated from the MCSL equation of state for the largest system studied at each density are given in Table III along with the values chosen for t_c. The fully corrected transport coefficients for a given volume follow from a linear least-squares fit to an expression linear in $1/N$ of the finite-N values of Table II, augmented by the appropriate long-time tail correction. The same values of N are used in each fit as were used in extrapolating the equation of state. The results for the thermal conductivity and shear viscosity are given in Table III and the mutual and thermal diffusion

coefficients are given in Table IV. The tables list separately the long-time tail contribution $\hat{L}_\alpha^{[2]}(t_c/t_0)$, as well as the Enskog value of the transport coefficient L_α^E, expressed in appropriate combinations of the mass unit m_1, the length unit σ_1, and the time unit $\sigma_1/\sqrt{m_1\beta}$, viz.

$$\tilde{L}_{\eta\eta}=\frac{(m_1\beta)^{1/2}\sigma_1^2}{m_1}L_{\eta\eta},$$

$$\tilde{L}_{uu}=\frac{(m_1\beta)^{3/2}\sigma_1^2}{m_1}L_{uu},$$

$$\tilde{L}_{u1}=\frac{(m_1\beta)^{1/2}\sigma_1^2}{m_1}L_{u1}, \tag{13}$$

$$\tilde{L}_{11}=\frac{\sigma_1^2}{m_1(m_1\beta)^{1/2}}L_{11}.$$

In each case we have confirmed the agreement between the time-correlation function $\rho_\alpha(t;N)$ for the largest N and the mode-coupling formula

TABLE IV. The mutual and thermal diffusion coefficients as functions of reduced volume V/V_0. The Monte Carlo and molecular-dynamics estimates, relative to the Enskog values, are $\hat{L}_\alpha$, with $\alpha=11$ for mutual diffusion and $\alpha=u1$ for thermal diffusion; $\hat{L}_\alpha^{[2]}(s_c)$ is the long-time tail contribution from the mode-coupling theory for the crossover time $t_c=s_c t_0$, given in Table III, $\tilde{L}_\alpha$ is the Enskog transport coefficient reduced as in Eq. (13). The numbers in parentheses are the standard deviations in the low-order digit.

| V/V_0	$\hat{L}_{11}$	$\hat{L}_{11}^{[1]}(s_c)$	$\tilde{L}_{11}^E$	$\hat{L}_{u1}$	$\hat{L}_{u1}^{[2]}(s_c)$	$\tilde{L}_{u1}^E$
1.7	0.7207(118)	0.0113	$5.122\,98\times10^{-4}$	0.7453(283)	0.0276	$-3.303\,08\times10^{-2}$
1.8	0.7821(73)	0.0115	$5.613\,18\times10^{-4}$	0.8144(135)	0.0257	$-3.650\,55\times10^{-2}$
1.9	0.7966(69)	0.0115	$6.068\,61\times10^{-4}$	0.8337(116)	0.0238	$-3.971\,18\times10^{-2}$
2	0.8301(69)	0.0113	$6.491\,79\times10^{-4}$	0.8492(112)	0.0220	$-4.267\,48\times10^{-2}$
2.4	0.8833(52)	0.0092	$7.912\,28\times10^{-4}$	0.8847(71)	0.0155	$-5.252\,92\times10^{-2}$
3	0.9199(67)	0.0061	$9.450\,71\times10^{-4}$	0.9284(80)	0.0091	$-6.307\,22\times10^{-2}$
5	0.9454(63)	0.0019	$1.213\,35\times10^{-3}$	0.9560(71)	0.0024	$-8.129\,49\times10^{-2}$
10	0.9747(59)	0.0004	$1.431\,44\times10^{-3}$	0.9767(68)	0.0005	$-9.597\,84\times10^{-2}$
20	0.9960(49)	0.0001	$1.545\,73\times10^{-3}$	0.9960(60)	0.0001	$-1.036\,26\times10^{-1}$
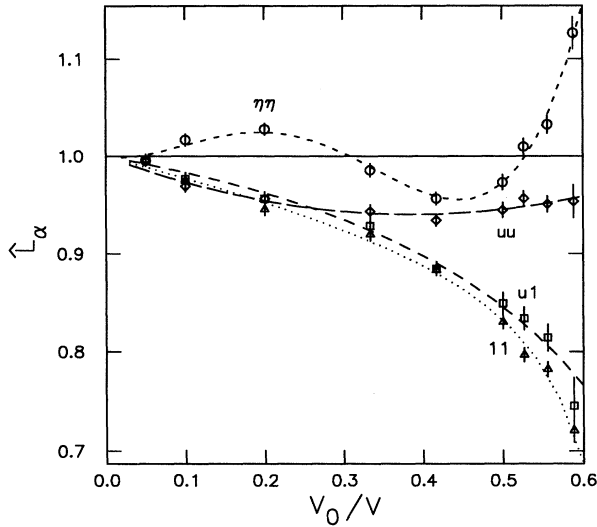
FIG. 4. Transport coefficients relative to the Enskog values $\hat{L}_\alpha$ as functions of reduced density V_0/V: $\alpha=11$ for the mutual diffusion, $\alpha=u1$ for the thermal diffusion, $\alpha=uu$ for the heat conductivity, and $\alpha=\eta\eta$ for the shear viscosity. The lines are rational function fits, Eq. (15). Statistical uncertainties are marked at plus or minus one standard deviation.

$$\rho_\alpha(t) \sim \frac{k_\alpha}{t^{3/2}} \qquad (14)$$

for t near t_c. In addition, we have confirmed that the final values reported for the infinite-system transport coefficients are insensitive to the exact choice of t_c.

The final estimates for the transport coefficients are shown as functions of density in Fig. 4. The data can be fit within the statistical uncertainties by rational functions in the density of degree 4 or less in the numerator and of degree 1 or less in the denominator,

$$\hat{L}_\alpha = \frac{1 + \sum_{j=1}^{4} a_i^{(\alpha)}(V_0/V)^i}{1 + b_1^{(\alpha)}(V_0/V)} , \qquad (15)$$

with the coefficients $a_i^{(\alpha)}, b_i^{(\alpha)}$ given in Table V. The fitting functions are displayed in Fig. 4.

V. DISCUSSION

The behavior of the pressure with system size reported in Fig. 1 for high densities implies serious consequences for the accurate determination of the equation of state

and the phase diagram by MC and MD calculation. The infinite-system correction to the pressure grows with density and extrapolation to the thermodynamic limit requires larger systems in order to achieve the $O(1/N)$ regime. Indeed for $V < 2V_0$ we see that 108- and 256-particle results imply a correction of the wrong sign. We note, however, that this effect is observed here not because the nonlinearity in $1/N$ is so large, but because the uncertainties are so small ($< 0.005\%$ for $N=1372$) that the second-order term can be seen. Similar nonlinearities are expected in the neighborhood of the coexistence region of a phase transition, but then on a much larger scale. We note that effects of a similar nature have been observed in single-component systems by Wood [41] for hard disks, by Erpenbeck and Wood [42,43] for hard spheres, and by Erpenbeck [44] for the (spline cutoff) Lennard-Jones potential near the triple point.

We also have observed a decrease in the $[\partial\Delta p/\partial(1/V)]_T$ near $1.8V_0$, for Δp the pressure less the MCSL pressure. Presumably this decrease presages one or more important phase transitions which occur at higher density. The suggestion that one treat this region with greater care appears particularly timely in view of recent theoretical suggestions of fluid phase demixing by Biben and Hansen [28] and Frenkel and Louis [29]. Clearly we have no evidence for such a phase transition over the density range studied here.

The corrections to the finite-system finite-time transport coefficients are quite a different matter than the equation of state. Comparing the "raw" values for $N=108$ from Table II with the fully corrected values in Tables III and IV, we see that these corrections grow from a few percent at low densities to nearly 10% for L_{uu} at $1.8V_0$. In the case of thermal transport coefficients of mutual diffusion, thermal diffusion, and thermal conduction, we observe that the difference between the infinite-system estimate and the $N=108$ value exceeds the statistical uncertainty for every density. Moreover, the long-time corrections $\hat{L}_\alpha^{[2]}(s_c)$ increase with increasing density, becoming comparable to the standard deviation for $V=3V_0$. For shear viscosity, the $1/N$ correction is seen to remain significant, but the long-time tail correction has a maximum near $V=5V_0$, decreasing in importance both at high and low density. The $1/N$ corrections remain of the order of 10% of the 108-particle result over the entire density range. At least in the present range of densities, there is little to suggest the presence of an enhancement to the viscosity from so-called "molasses" tails, i.e., long-time tails in the cross and potential contributions to the

TABLE V. The coefficients $a_i^{(\alpha)}$ and $b_i^{(\alpha)}$ of the fitting rational polynomial, Eq. (15), for the each of the four transport coefficients: $\alpha=11$ for mutual diffusion, $\alpha=u1$ for thermal diffusion, $\alpha=uu$ for thermal conduction, and $\alpha=\eta\eta$ for shear viscosity. The goodness of each fit is indicated by χ^2, with ν degrees of freedom.

α	$b_1^{(\alpha)}$	$a_1^{(\alpha)}$	$a_2^{(\alpha)}$	$a_3^{(\alpha)}$	$a_4^{(\alpha)}$	χ^2	ν
11	−1.459 21	−1.680 92	0.261 37			9.3	6
$u1$	−1.021 56	−1.172 65				5.1	7
uu		−0.310 51	0.401 77			6.5	7
$\eta\eta$		−0.148 39	4.331 41	−19.255	21.928	6.5	5

viscosity autocorrelation function, as has been seen in single-component fluids [45–47]. It seems likely, however, that such effects will only appear at higher densities; calculations for $V < 1.7V_0$ aimed at elucidating the high-density equation of state as well as the behavior of the transport coefficients are currently in progress.

Finally, for the interested reader, we note that the present calculations which were performed on a variety of computer hardware required very substantial blocks of computer time. The $3V_0$ calculations were run on CRAY-YMP machines, using single-precision floating-point arithmetic (48-bit fractional part) for both the Monte Carlo and molecular dynamics, requiring 315 h of CPU time. The remainder of the calculations were performed on various SUN-4 SPARC workstations (includ-

ing SUN-4/300 and SparcStation 1, 1+, IPC, and 2) using double-precision floating point (53-bit fractional part), requiring a total of 680 days of CPU time. Clearly, very substantial computational resources are needed to evaluate the transport coefficients to an accuracy of less than 1%.

[1] D. Enskog, Kungl. Svenska Vet.-Akad. Handl. **63**, 4 (1922).
[2] S. Chapman and T. G. Cowling, *The Mathematical Theory of Nonuniform Gases*, 3rd ed. (Cambridge University Press, Cambridge, 1970).
[3] J. Weinstock, Phys. Rev. **140A**, 460 (1965).
[4] J. R. Dorfman and E. G. D. Cohen, Phys. Lett. **16**, 124 (1965).
[5] J. R. Dorfman and E. G. D. Cohen, Phys. Rev. A **6**, 776 (1972).
[6] J. R. Dorfman and E. G. D. Cohen, Phys. Rev. A **12**, 292 (1975).
[7] J. V. Sengers, D. T. Gillespie, and J. J. Perez-Esandi, Physica **90A**, 365 (1978).
[8] B. Kamgar-Parsi and J. V. Sengers, Phys. Rev. Lett. **51**, 2163 (1983).
[9] M. H. Ernst, E. H. Hauge, and J. M. J. van Leeuwen, Phys. Rev. A **4**, 2055 (1971).
[10] M. H. Ernst, E. H. Hauge, and J. M. J. van Leeuwen, J. Stat. Phys. **15**, 7 (1976).
[11] J. J. Erpenbeck, Phys. Rev. A **39**, 4718 (1989).
[12] J. J. Erpenbeck, Phys. Rev. A **45**, 2298 (1992).
[13] H. van Beijeren and M. H. Ernst, Physica **68**, 437 (1973).
[14] H. van Beijeren and M. H. Ernst, Physica **70**, 225 (1973).
[15] M. Lopez de Haro, E. G. D. Cohen, and J. M. Kincaid, J. Chem. Phys. **78**, 2746 (1983).
[16] J. M. Kincaid, M. Lopez de Haro, and E. G. D. Cohen, J. Chem. Phys. **79**, 4509 (1983).
[17] M. Lopez de Haro and E. G. D. Cohen, J. Chem. Phys. **80**, 408 (1984).
[18] J. M. Kincaid, E. G. D. Cohen, and M. Lopez de Haro, J. Chem. Phys. **86**, 937 (1987).
[19] E. B. Smith and K. R. Lea, Trans. Faraday Soc. **59**, 1535 (1963).
[20] B. J. Adler, J. Chem. Phys. **40**, 2724 (1964).
[21] L. L. Lee and D. Levesque, Mol. Phys. **26**, 1351 (1973).
[22] P. H. Fries and J. P. Hansen, Mol. Phys. **48**, 891 (1983).
[23] G. Jackson, J. S. Rowlinson, and F. van Swol, J. Phys. Chem. **91**, 4907 (1987).
[24] W. G. Kranendonk and D. Frenkel, Mol. Phys. **72**, 679

(1991).
[25] W. G. Kranendonk and D. Frenkel, Mol. Phys. **72**, 715 (1991).
[26] J. L. Lebowitz, Phys. Rev. **133**, A895 (1964).
[27] J. L. Lebowitz and J. S. Rowlinson, J. Chem. Phys. **41**, 133 (1964).
[28] T. Biben and J. P. Hansen, Phys. Rev. Lett. **66**, 2215 (1991).
[29] D. Frenkel and A. A. Louis, Phys. Rev. Lett. **68**, 3363 (1992).
[30] G. A. Mansoori, N. F. Carnahan, K. E. Starling, and T. W. Leland, J. Chem. Phys. **54**, 1523 (1971).
[31] T. M. Reed and K. E. Gubbins, *Applied Statistical Mechanics* (McGraw-Hill, New York, 1973).
[32] W. J. Kennedy and J. E. Gentile, *Statistical Computing* (Dekker, New York, 1980).
[33] A. M. Ferrenberg, D. P. Landau, and Y. J. Wong, Phys. Rev. Lett. **69**, 3382 (1992).
[34] W. W. Wood, J. Chem. Phys. **48**, 415 (1968).
[35] J. J. Erpenbeck and W. W. Wood, in *Modern Theoretical Chemistry, Vol. 6, Statistical Mechanics, Part B, Time Dependent Processes*, edited by B. J. Berne (Plenum, New York, 1977), p. 1.
[36] T. Kihara, Nippon-Sugaku-Buturigakukaisi **17**, 11 (1943).
[37] J. O. Hirschfelder, C. F. Curtiss, and R. B. Bird, *Molecular Theory of Gases and Liquids* (Wiley, New York, 1954).
[38] M. Rigby and E. B. Smith, Trans. Faraday Soc. **59**, 2469 (1963).
[39] Y. Pomeau, J. Chem. Phys. **57**, 2800 (1972).
[40] W. W. Wood, J. Stat. Phys. **57**, 675 (1989).
[41] W. W. Wood, J. Chem. Phys. **52**, 729 (1970).
[42] J. J. Erpenbeck and W. W. Wood, J. Stat. Phys. **35**, 321 (1984).
[43] J. J. Erpenbeck and W. W. Wood, J. Stat. Phys. **40**, 787 (1985).
[44] J. J. Erpenbeck, Phys. Rev. A **35**, 218 (1987).
[45] B. J. Alder, Physica **108A**, 413 (1983).
[46] D. J. Evans, J. Stat. Phys. **22**, 81 (1980).
[47] J. J. Erpenbeck and W. W. Wood, J. Stat. Phys. **24**, 455 (1981).